Rapid Communications

Valence bond solid and possible deconfined quantum criticality in an extended kagome lattice Heisenberg antiferromagnet

Alexander Wietek [1,*] and Andreas M. Läuchli [2]

[1] *Center for Computational Quantum Physics, Flatiron Institute, 162 5th Avenue, New York, New York 10010, USA*

[2] *Institut für Theoretische Physik, Universität Innsbruck, A-6020 Innsbruck, Austria*

(Received 28 August 2019; revised 31 March 2020; accepted 14 July 2020; published 27 July 2020)

We present numerical evidence for the existence of an extended valence bond solid (VBS) phase at $T = 0$ in the kagome $S = 1/2$ Heisenberg antiferromagnet with ferromagnetic further-neighbor interactions. The VBS is located at the boundary between two magnetically ordered regions and extends close to the nearest-neighbor Heisenberg point. It exhibits a diamondlike singlet covering pattern with a 12-site unit cell. Our results suggest the possibility of a direct, possibly continuous, quantum phase transition from the neighboring $\mathbf{q} = 0$ coplanar magnetically ordered phase into the VBS phase. Moreover, a second phase which breaks lattice symmetries, and is of likely spin-nematic type, is found close to the transition to the ferromagnetic phase. The results have been obtained using large-scale numerical exact diagonalization. We discuss implications of our results on the nature of the nearest-neighbor Heisenberg antiferromagnet.

DOI: 10.1103/PhysRevB.102.020411

Introduction. We expect the unexpected when strong electron interactions meet geometric frustration. The emergence of novel exotic states of matter in frustrated quantum magnets is intensely studied in experiments, theory, and numerical computations. Several materials and theoretical models exhibit a lack of magnetic ordering even at lowest temperatures. Instead, genuine quantum many-body states, such as quantum spin liquids [1,2] or valence bond solids (VBS) can be observed [3–7]. Several experiments also have given evidence for emerging VBS phases in a variety of materials [8–11].

The nearest-neighbor kagome lattice Heisenberg spin-1/2 antiferromagnet arguably remains one of the most puzzling conundrums in frustrated magnetism. Various scenarios on the nature of its ground state have been proposed. It has been found early on, that a VBS is energetically competitive [12–16]. However, more recent numerical studies suggest that different spin disordered states are a more likely scenario. Several density-matrix renormalization group studies later suggested the possibility of a gapped spin liquid ground state [17,18]. More recently, variational Monte Carlo and tensor network studies also suggested a gapless spin liquid state being realized [19–24]. While a conclusion on the nature of its ground state has not unanimously been reached to date [25], several exotic new states of matter have been clearly identified in close proximity to the nearest-neighbor model [26–29]. Among those, a chiral spin liquid has been found in an extended Heisenberg model with antiferromagnetic second and third nearest-neighbor interactions [27–29]. The classical ground-state phase diagram of this model has previously been established [30,31]. A phase transition between two magnetic orders has been found for antiferromagnetic interactions. In the quantum case, the chiral spin liquid phase is located along the transition line between these two magnetic phases and extends close to the nearest-neighbor point. The classical phase diagram also contains a phase transition line between two types of coplanar magnetic orders for *ferromagnetic* second and third nearest-neighbor interactions. Given that some frustrated kagome materials involving both ferromagnetic and antiferromagnetic couplings are known to exist [32–34], there is a strong interest to explore whether novel phases also emerge at or in the vicinity of the classical transition line at $J_3 = 2J_2 < 0$.

Here, we investigate the kagome spin-1/2 Heisenberg antiferromagnet with additional ferromagnetic second and third nearest-neighbor interactions. We present conclusive numerical evidence for the appearance of a *diamond* VBS phase in an extended parameter range. The VBS phase is located in the vicinity of the classical transition line between the $\mathbf{q} = 0$ and $\sqrt{3} \times \sqrt{3}$ magnetic orders. Interestingly, the phase extends close up to the nearest-neighbor Heisenberg point.

Model and phase diagram. We consider the Hamiltonian

$$H = J_1 \sum_{\langle i,j \rangle} \vec{S}_i \cdot \vec{S}_j + J_2 \sum_{\langle\langle i,j \rangle\rangle} \vec{S}_i \cdot \vec{S}_j + J_3 \sum_{\langle\langle\langle i,j \rangle\rangle\rangle_{\mathrm{h}}} \vec{S}_i \cdot \vec{S}_j, \tag{1}$$

on a kagome lattice geometry, where $\vec{S}_i = (S_i^x, S_i^y, S_i^z)$ denotes spin-1/2 operators, $\langle \cdots \rangle$ and $\langle\langle \cdots \rangle\rangle$ denote the sum over nearest- and second-nearest-neighbor sites, and $\langle\langle\langle \cdots \rangle\rangle\rangle_{\mathrm{h}}$ denotes the sum over third-nearest-neighbor interactions only across the hexagons of the kagome lattice [cf. Fig. 1(b)]. In the following, we set $J_1 = 1$ and focus on the case of ferromagnetic couplings $J_2 < 0$ and $J_3 < 0$.

Most of our results are obtained by exact diagonalization (ED) calculations on a $N = 36$-site kagome lattice with periodic boundary conditions [35,36]. Its Brillouin zone

*awietek@flatironinstitute.org

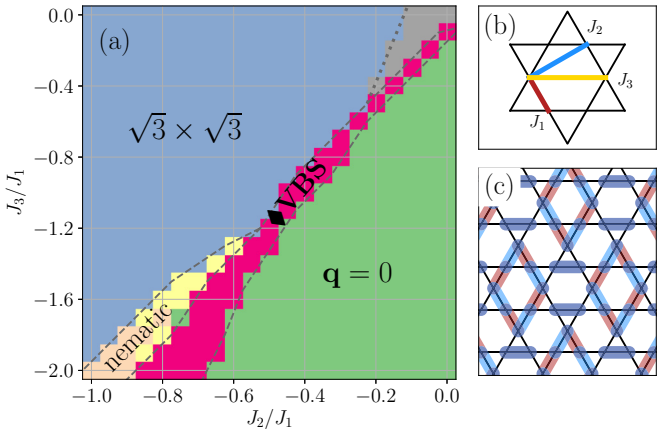

FIG. 1. (a) Approximate phase diagram of the extended kagome Heisenberg model Eq. 1 for $J_1 > 0$ and $J_2, J_3 \leqslant 0$ as obtained from ED on a 36-site simulation cluster. Between two regions of magnetic $\mathbf{q} = 0$ and $\sqrt{3} \times \sqrt{3}$ order a diamond VBS and a spin-nematic phase are emerging. Different colors denote the quantum numbers of the first excited state. Green: $S = 1$, Γ.D6.A2 or Γ.D6.E2. Blue: $S = 1$, Γ.D6.B1 or K.D3.A1. Pink: $S = 0$, M.D2.A2. Orange: $S = 0$, M.D2.A1. Yellow: $S = 2$, Γ.D6.A1. Gray: $S = 0$, various space group sectors. Gray lines are a guide to the eye. (b) Coupling geometry for the Hamiltonian Eq. 1. (c) Structure of the diamond VBS with a 12-site unit cell. Dimer coverings on the diamond structure are in resonance.

features the **K** and **M** points and is hence suited to stabilize both the $\sqrt{3} \times \sqrt{3}$ and $\mathbf{q} = 0$ order. Selected results have been obtained on smaller clusters as well as on the larger $N = 48$ cluster [25,35]. We detect ordering by investigating suitably chosen order parameters and performing tower-of-states analysis, i.e., comparing quantum numbers of finite-size energy eigenstates with theoretical predictions. The order parameters of the ground state and finite-size energy spectra are calculated on a grid for $J_2 \in [-1, 0]$ with spacing 0.05 and $J_3 \in [-2, 0]$ with spacing 0.1.

For classical Heisenberg spins the phase diagram of this model has been established in Ref. [31]. The $\sqrt{3} \times \sqrt{3}$ magnetic phase is separated from the $\mathbf{q} = 0$ magnetic phase by a transition line located at $J_3 = 2J_2$. For $J_3 < -2$ and $J_2 < -1$ a ferromagnetic state is stabilized.

In Fig. 1 we present a first exploration of the quantum ($S = 1/2$) phase diagram based on a map organized by the quantum numbers of the first excitation above the ground state. The assignment of the phases is performed based on a tower-of-states analysis for different candidate phases. According to this rationale, the blue region indicates the $\sqrt{3} \times \sqrt{3}$ magnetic order, the green region indicates the $\mathbf{q} = 0$ magnetic order, and the pink region the VBS phase. The nematic phase extends in the yellow and orange region, where two different quantum numbers are the first excitation. The gray lines serve as a guide to the eye and determine approximate phase boundaries. Apart from the expected $\sqrt{3} \times \sqrt{3}$ and $\mathbf{q} = 0$ coplanar magnetic order phases, we find an unanticipated diamond VBS and a lattice symmetry breaking spin-nematic phase located in the vicinity of the classical transition line. In Fig. 2 we corroborate the spectroscopy picture with an analysis of corresponding order parameters. The spin-nematic phase extends close to the classical ferromagnetic phase, while the VBS phase extends close to the nearest-neighbor point. We now proceed to characterize the reported phases in more detail.

Magnetic order. The $\mathbf{q} = 0$ and $\sqrt{3} \times \sqrt{3}$ magnetic phases break spin rotational SU(2) symmetry and exhibit patterns of magnetic ordering shown in the Supplemental Material [37]. We consider the static spin structure factor,

$$S(\mathbf{q}) = \frac{1}{N} \sum_{k,l=1}^{N} e^{-i\mathbf{q}\cdot(\mathbf{r}_k - \mathbf{r}_l)} \langle \vec{S}_k \cdot \vec{S}_l \rangle. \tag{2}$$

For the two magnetic orders, the structure factor is peaked at the points

$$\mathbf{M}' = (2\pi, 2\pi/\sqrt{3}) \quad \text{for } \mathbf{q} = 0 \text{ order}, \tag{3}$$

$$\mathbf{K}' = (8\pi/3, 0) \quad \text{for } \sqrt{3} \times \sqrt{3} \text{ order}, \tag{4}$$

in the extended Brillouin zone (cf. [30]). Hence, $S(\mathbf{M}')$ and $S(\mathbf{K}')$ shown in Figs. 2(a) and 2(b) identify both magnetic phases, respectively. The regions where these structure factors are peaked coincide with the blue and green regions in Fig. 1.

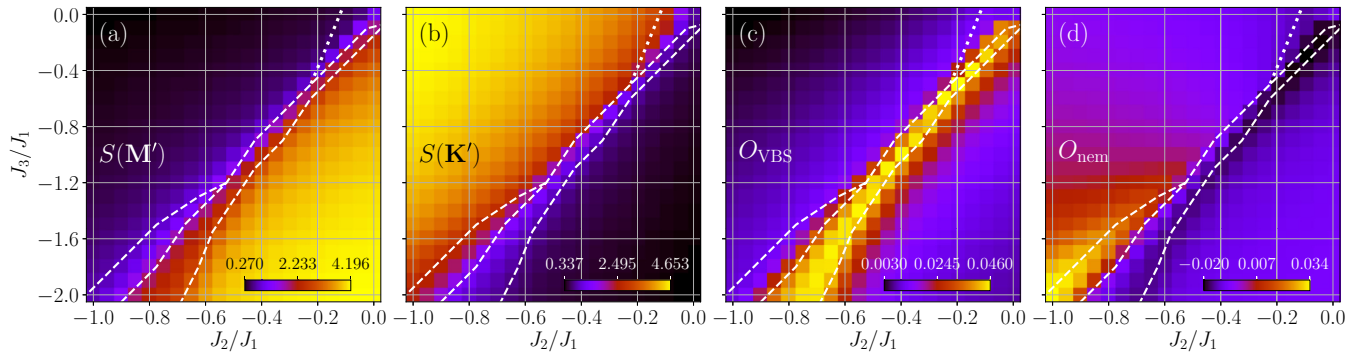

FIG. 2. ED results on a 36-site simulation cluster: (a) Spin structure factor $S(\mathbf{M}')$ evaluated at $\mathbf{M}' = (2\pi, 2\pi/\sqrt{3})$, indicating $\mathbf{q} = 0$ magnetic order. (b) Spin structure factor $S(\mathbf{K}')$ evaluated at $\mathbf{K}' = (8\pi/3, 0)$, indicating $\sqrt{3} \times \sqrt{3}$ magnetic order. (c) Diamond VBS order parameter O_{VBS} as defined in Eq. 7. A diamond VBS phase is emerging in between the two magnetic orders. (d) Nematic phase order parameter O_{nem} as defined in Eq. 8, indicating the extent of the plaquette-nematic phase. Note the good agreement between the order parameter inferred phase diagram and the excited state spectroscopy phase diagram of Fig. 1 indicated with the dashed white lines.

The blue region in Fig. 1(a) is given by the points, where the first excitation is a triplet, $S = 1$, state with K.D3.A1 or Γ.D6.B1 space group quantum numbers [37,38]. In the green region in Fig. 1(a), the triplet states, $S = 1$, with Γ.D6.A2 and Γ.D6.E2 space group quantum numbers are the first excitation. Thus, the spin structure factor and energy spectroscopy yield consistent results on the extent of these two phases.

Diamond VBS phase. To identify the VBS and the lattice symmetry breaking spin-nematic phase we consider the connected dimer correlations,

$$D_{kl} \equiv \langle (\vec{S}_k \cdot \vec{S}_l)(\vec{S}_1 \cdot \vec{S}_0) \rangle - \langle \vec{S}_k \cdot \vec{S}_l \rangle \langle \vec{S}_1 \cdot \vec{S}_0 \rangle, \tag{5}$$

where the sites 0 and 1 are an arbitrary nearest-neighbor bond chosen as reference. These correlations are long-ranged in the VBS phase and exhibit specific patterns of positive and negative correlation that can be predicted for the model VBS state. For the 48-site cluster we computed the diagonal S^z-dimer correlations

$$D^z_{kl} \equiv \left\langle \left(S^z_k S^z_l\right)\left(S^z_1 S^z_0\right)\right\rangle - \left\langle S^z_k S^z_l\right\rangle \left\langle S^z_1 S^z_0\right\rangle. \tag{6}$$

The sign structure of these correlations serves as a first fingerprint of the particular VBS phase realized. For the diamond VBS state the expected sign structure of the dimer correlations is shown in [37]. Thereby, we define an order parameter of the VBS phase,

$$O_{\mathrm{VBS}} \equiv \frac{1}{N} \sum_{\langle k,l \rangle} \theta^{\mathrm{VBS}}_{kl} D_{kl}, \tag{7}$$

where $\theta^{\mathrm{VBS}}_{kl} = \pm 1$ denotes the sign as defined in the Supplemental Material.

This diamond VBS parameter O_{VBS} is shown in Fig. 2(c), indicating the extent of the VBS phase. It is located between the two magnetic orders and extends basically along the whole classical transition line from $J_2 = -1$ to $J_2 = 0$. The region of pronounced O_{VBS} also coincides with the pink region in Fig. 1. There, the first excited state is a singlet $S = 0$ state with M.D2.A2 space group quantum number.

The precise nature of the reported VBS itself requires some more care. There are two basic candidate VBS model states with a 12-site unit cell [17,39–41]. A pinwheel VBS, where all dimers are static and the pinwheels all share the same orientation. This particular state is eightfold degenerate, a factor 4 from the translations and a factor 2 from the pinwheel orientation. On the other hand, like in many other VBS scenarios, there is a resonant version of this VBS, where we consider resonances involving eight-site loops in the shape of a diamond lozenge. A fully packed state of nonoverlapping resonances is shown in Fig. 1(c). This state is actually 12-fold degenerate, a factor 4 from the translations, and a factor 3 from the orientations of the diamond lozenges. The dimer-dimer correlations in these two model states are identical, so that dimer correlations alone cannot distinguish the two states. However, the spectral decomposition [37] reveals that beyond some common levels the diamond VBS features a characteristic spin singlet Γ.D6.E2 level, while the pinwheel VBS comes with a characteristic Γ.D6.A2 level. A close inspection of the energy spectrum of the VBS phase in Figs. 3(a) and 3(c) reveals a low-lying spin singlet Γ.D6.E2 level, and

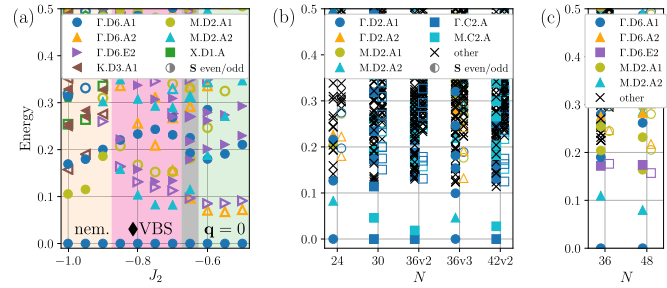

FIG. 3. Diamond VBS: (a) Energy spectra with quantum numbers for $J_3 = -2$ and $S_z = 0$. Different colors and symbols denote different quantum numbers. Full (empty) symbols denote even (odd) spin-flip symmetry eigenstates. The spin-nematic phase extends up to $J_2 \lesssim -0.9$ (orange shaded region). The first excited level is a singlet with space group quantum number M.D2.A1. The diamond VBS phase exists in the window (pink shaded region) $-0.9 \lesssim J_2 \lesssim -0.7$. The first excited state is a singlet with space group quantum number M.D2.A2. Beyond, the $\mathbf{q} = 0$ is stabilized with triplet excitations (green shaded region). The narrow gray shaded region highlights the putative quantum critical Néel-VBS transition. (b) Energy spectra as a function of system size for $J_2 = -0.16$ and $J_3 = -0.4$. The lowest excited level on all lattices is a singlet with momentum M. For a description of the used clusters, cf. Ref. [36]. (c) Energy spectra for the C_{6v} symmetric 36- and 48-site clusters at $J_2 = -0.16$ and $J_3 = -0.4$. The lowest excited states again have the same M momentum and space group sector.

the absence of a low-lying Γ.D6.A2 level, thus clarifying the presence of a *diamond* VBS phase in this parameter region.

The spectral features of the VBS phase can be detected across various system sizes from $N = 24$ to $N = 48$ (only selected sectors) as shown in Fig. 3. The lowest excited state on all clusters we studied belongs to the same M momentum and space group sector, consistent with the diamond VBS order in the thermodynamic limit. Hence, the evidence for a VBS is not only robust in the dimer correlations in Fig. 4 for system sizes $N = 36$ and $N = 48$ but also in the energy spectra for all system sizes we studied.

Spin-nematic-plaquette phase. The dimer correlations also exhibit a different peculiar sign structure in another parameter region, as shown for $J_2 = -1$ and $J_3 = -2$ in Fig. 5(a). We see characteristic positively correlated hexagon patterns suggest-

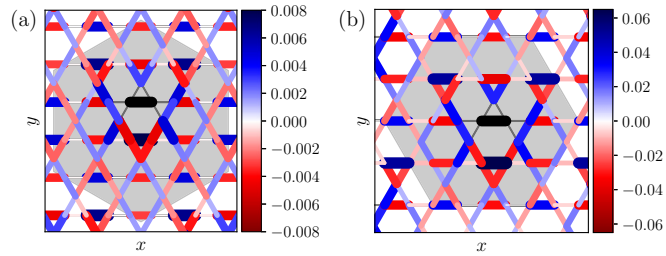

FIG. 4. Ground-state dimer correlations in the VBS phase for $J_2/J_1 = -0.4$, $J_3/J_1 = -0.9$ from exact diagonalization. (a) S^z dimer-dimer correlations D^z_{kl} as defined in Eq. (6) on the 48-site cluster. (b) Dimer-dimer correlations D_{kl} as defined in Eq. (5) on the 36-site cluster. The black line is used as the reference bond and the gray area shows the Wigner-Seitz simulation cell.

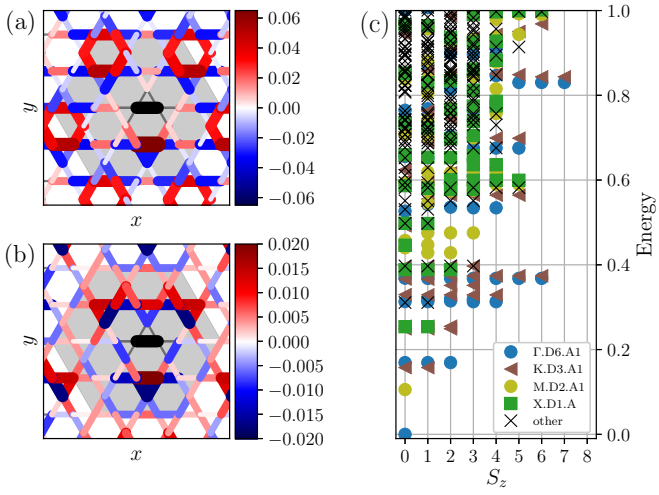

FIG. 5. Characterization of a possibly spin-nematic phase. (a) Observed ground-state dimer-dimer correlations D_{kl} in the nematic phase for $J_2/J_1 = -1$, $J_3/J_1 = -2$ as defined in Eq. 5. Red (blue) corresponds to positive (negative) correlation. The black line is used as the reference bond and the gray area shows the 36-site simulation cell. (b) Quadrupolar ground-state correlations Q_{kl} as defined in Eq. 9 showing hexagon-ring sign structure. (c) Energy spectrum for $J_2 = -1, J_3 = -2$ in the nematic phase for $S_z < 9$. The degeneracy at different S_z gives total spin quantum number S. Odd-S sectors are not present in the low-energy tower of states, indicating a quadrupolar spin-nematic phase.

ing a 2×2 unit cell superstructure. However, we are unaware of a *singlet* VBS model state exhibiting such a correlation pattern. We analogously define an order parameter for this lattice symmetry breaking pattern,

$$O_{\text{nem}} \equiv \frac{1}{N} \sum_{\langle k,l \rangle} \theta_{kl}^{\text{nem}} D_{kl}, \tag{8}$$

where the sign $\theta_{kl}^{\text{nem}} = \pm 1$ is defined in the Supplemental Material. The region in parameter space where its signal is strong is shown in Fig. 1(d).

Since we are unaware of a singlet VBS with this structure, and due to the vicinity of the ferromagnet, we explore the possibility of a phase with additional spin-nematic character, for example of quadrupolar type [42]. Several examples of frustrated ferromagnets giving rise to spin-nematic phases have been discussed [34,43–46]. In Fig. 5(b) we display the quadrupolar bond correlations,

$$Q_{kl} \equiv \langle (S_k^+ S_l^+)(S_1^- S_0^-) \rangle, \tag{9}$$

exhibiting sizable correlations. We notice a peculiar hexagon-ring sign structure, where the correlations on hexagons surrounding the middle hexagon are negative, while correlations on the other hexagons are positive. In Fig. 5(c) we show an energy spectrum resolved by total S^z and we can see a low-lying $S = 2$ level, which could be due to the quadrupolar character. The lowest singlet excited state is a M.D2.A1 level, which is in agreement with the reported 2×2 hexagon plaquette superstructure. So we see quite strong evidence for a novel phase, distinct from the other reported phases, but a detailed characterization of the phase (e.g., a corroboration of the spin-nematic character) has to be left for future research.

Discussion and outlook. We have explored the appearance of two unexpected phases along the classical transition line in the $S = 1/2$ kagome Heisenberg antiferromagnet with competing ferromagnetic further neighbor couplings. The first phase is a *diamond* VBS with a 12-site unit cell. This VBS or variants thereof have been seen in quantum dimer models [16,40,41,47,48] and hinted at by fluctuations or weak correlations in quantum spin models at the nearest-neighbor point ($J_2 = J_3 = 0$) in Refs. [17,25]. We have now firmly established this VBS phase in the extended model (1). The location of this VBS phase in the immediate vicinity of the $\mathbf{q} = 0$ magnetic order, and the apparent second-order nature of the phase transition between the two phases in exact diagonalization, places this transition into a contender role for an example of a deconfined quantum critical transition, with possibly deconfined spin excitations at the transition [49]. Recent analytical work on the triangular lattice [50] and the analysis of the matching VBS and Néel monopoles in the Dirac spin liquid [51] combined with our numerical results renders this scenario at least plausible. It will also be important to work out the connection between the VBS phase and the Dirac spin liquid state, which is currently a prime candidate to describe the kagome antiferromagnet at small antiferromagnetic J_2 coupling [19,21–24], before entering the $\mathbf{q} = 0$ magnetic ordered phase.

This part of the phase diagram is then separated by a likely first-order phase transition from the $\sqrt{3} \times \sqrt{3}$ magnetically ordered phase and the lattice symmetry breaking spin-nematic phase close to the ferromagnetic phase. The precise nature of the latter phase is left for future studies.

Acknowledgments. We acknowledge useful discussions with Y.-C. He, G. Misguich, and C. Wang. The Flatiron Institute is a division of the Simons Foundation. We thank the Austrian Science Fund FWF for support within the project DFG-FOR1807 (I-2868). This research was supported in part by Perimeter Institute for Theoretical Physics. Research at Perimeter Institute is supported by the Government of Canada through the Department of Innovation, Science, and Economic Development, and by the Province of Ontario through the Ministry of Research and Innovation. The computational results presented have been achieved in part using the HPC infrastructure LEO of the University of Innsbruck. The computational results presented have been achieved in part using the Vienna Scientific Cluster (VSC). We acknowledge PRACE for granting access to "Joliot Curie" HPC resources at TGCC/CEA under Grant No. 2019204846.

[1] L. Balents, Spin liquids in frustrated magnets, Nature (London) **464**, 199 (2010).

[2] L. Savary and L. Balents, Quantum spin liquids: A review, Rep. Prog. Phys. **80**, 016502 (2016).

[3] C. K. Majumdar and D. K. Ghosh, On next-nearest-neighbor interaction in linear chain. I, J. Math. Phys. **10**, 1388 (1969).

[4] J.-B. Fouet, M. Mambrini, P. Sindzingre, and C. Lhuillier, Planar pyrochlore: A valence-bond crystal, Phys. Rev. B **67**, 054411 (2003).

[5] M. Mambrini, A. Läuchli, D. Poilblanc, and F. Mila, Plaquette valence-bond crystal in the frustrated Heisenberg quantum antiferromagnet on the square lattice, Phys. Rev. B **74**, 144422 (2006).

[6] M. E. Zhitomirsky and K. Ueda, Valence-bond crystal phase of a frustrated spin-1/2 square-lattice antiferromagnet, Phys. Rev. B **54**, 9007 (1996).

[7] Y. Iqbal, F. Becca, and D. Poilblanc, Valence-bond crystal in the extended kagome spin-$\frac{1}{2}$ quantum Heisenberg antiferromagnet: A variational Monte Carlo approach, Phys. Rev. B **83**, 100404(R) (2011).

[8] K. Matan, T. Ono, Y. Fukumoto, T. J. Sato, J. Yamaura, M. Yano, K. Morita, and H. Tanaka, Pinwheel valence-bond solid and triplet excitations in the two-dimensional deformed kagome lattice, Nat. Phys. **6**, 865 (2010).

[9] C. Rüegg, A pinwheel without wind, Nat. Phys. **6**, 837 (2010).

[10] J. P. Sheckelton, J. R. Neilson, D. G. Soltan, and T. M. McQueen, Possible valence-bond condensation in the frustrated cluster magnet $LiZn_2Mo_3O_8$, Nat. Mater. **11**, 493 (2012).

[11] R. W. Smaha, W. He, J. M. Jiang, C. J. Titus, J. Wen, Y.-F. Jiang, J. P. Sheckelton, C. J. Titus, S. G. Wang, Y.-S. Chen, S. J. Teat, A. A. Aczel, Y. Zhao, G. Xu, J. W. Lynn, H.-C. Jiang, and Y. S. Lee, Materializing rival ground states in the barlowite family of kagome magnets: Quantum spin liquid, spin ordered, and valence bond crystal states, npj Quantum Mater. **5**, 23 (2020).

[12] J. B. Marston and C. Zeng, Spin-Peierls and spin-liquid phases of kagomé quantum antiferromagnets, J. Appl. Phys. **69**, 5962 (1991).

[13] P. W. Leung and V. Elser, Numerical studies of a 36-site kagome antiferromagnet, Phys. Rev. B **47**, 5459 (1993).

[14] P. Nikolic and T. Senthil, Physics of low-energy singlet states of the kagome lattice quantum Heisenberg antiferromagnet, Phys. Rev. B **68**, 214415 (2003).

[15] R. R. P. Singh and D. A. Huse, Ground state of the spin-1/2 kagome-lattice Heisenberg antiferromagnet, Phys. Rev. B **76**, 180407(R) (2007).

[16] S. Capponi, V. R. Chandra, A. Auerbach, and M. Weinstein, *p*6 chiral resonating valence bonds in the kagome antiferromagnet, Phys. Rev. B **87**, 161118(R) (2013).

[17] S. Yan, D. A. Huse, and S. R. White, Spin-liquid ground state of the $S = 1/2$ Kagome Heisenberg antiferromagnet, Science **332**, 1173 (2011).

[18] S. Depenbrock, I. P. McCulloch, and U. Schollwöck, Nature of the Spin-Liquid Ground State of the $S = 1/2$ Heisenberg Model on the Kagome Lattice, Phys. Rev. Lett. **109**, 067201 (2012).

[19] Y. Ran, M. Hermele, P. A. Lee, and X.-G. Wen, Projected-Wave-Function Study of the Spin-1/2 Heisenberg Model on the Kagomé Lattice, Phys. Rev. Lett. **98**, 117205 (2007).

[20] Y. Iqbal, D. Poilblanc, and F. Becca, Spin-$\frac{1}{2}$ Heisenberg J_1-J_2 antiferromagnet on the kagome lattice, Phys. Rev. B **91**, 020402(R) (2015).

[21] Y. Iqbal, F. Becca, and D. Poilblanc, Projected wave function study of $\mathbb{Z}_2$ spin liquids on the kagome lattice for the spin-$\frac{1}{2}$ quantum Heisenberg antiferromagnet, Phys. Rev. B **84**, 020407(R) (2011).

[22] Y. Iqbal, F. Becca, S. Sorella, and D. Poilblanc, Gapless spin-liquid phase in the kagome spin-$\frac{1}{2}$ Heisenberg antiferromagnet, Phys. Rev. B **87**, 060405(R) (2013).

[23] Y.-C. He, M. P. Zaletel, M. Oshikawa, and F. Pollmann, Signatures of Dirac Cones in a DMRG Study Of The Kagome Heisenberg Model, Physi. Rev. X **7**, 031020 (2017).

[24] H. J. Liao, Z. Y. Xie, J. Chen, Z. Y. Liu, H. D. Xie, R. Z. Huang, B. Normand, and T. Xiang, Gapless Spin-Liquid Ground State in the $s = 1/2$ Kagome Antiferromagnet, Phys. Rev. Lett. **118**, 137202 (2017).

[25] A. M. Läuchli, J. Sudan, and R. Moessner, $S = \frac{1}{2}$ kagome Heisenberg antiferromagnet revisited, Phys. Rev. B **100**, 155142 (2019).

[26] B. Bauer, L. Cincio, B. P. Keller, M. Dolfi, G. Vidal, S. Trebst, and A. W. W. Ludwig, Chiral spin liquid and emergent anyons in a kagome lattice Mott insulator, Nat. Commun. **5**, 5137 (2014).

[27] S.-S. Gong, W. Zhu, and D. N. Sheng, Emergent chiral spin liquid: Fractional quantum Hall effect in a kagome Heisenberg model, Sci. Rep. **4**, 6317 (2014).

[28] A. Wietek, A. Sterdyniak, and A. M. Läuchli, Nature of chiral spin liquids on the kagome lattice, Phys. Rev. B **92**, 125122 (2015).

[29] Y.-C. He, D. N. Sheng, and Y. Chen, Chiral Spin Liquid in a Frustrated Anisotropic Kagome Heisenberg Model, Phys. Rev. Lett. **112**, 137202 (2014).

[30] L. Messio, C. Lhuillier, and G. Misguich, Lattice symmetries and regular magnetic orders in classical frustrated antiferromagnets, Phys. Rev. B **83**, 184401 (2011).

[31] L. Messio, B. Bernu, and C. Lhuillier, Kagome Antiferromagnet: A Chiral Topological Spin Liquid? Phys. Rev. Lett. **108**, 207204 (2012).

[32] B. Fåk, E. Kermarrec, L. Messio, B. Bernu, C. Lhuillier, F. Bert, P. Mendels, B. Koteswararao, F. Bouquet, J. Ollivier, A. D. Hillier, A. Amato, R. H. Colman, and A. S. Wills, Kapellasite: A Kagome Quantum Spin Liquid with Competing Interactions, Phys. Rev. Lett. **109**, 037208 (2012).

[33] E. Kermarrec, A. Zorko, F. Bert, R. H. Colman, B. Koteswararao, F. Bouquet, P. Bonville, A. Hillier, A. Amato, J. van Tol, A. Ozarowski, A. S. Wills, and P. Mendels, Spin dynamics and disorder effects in the $s = \frac{1}{2}$ kagome Heisenberg spin-liquid phase of kapellasite, Phys. Rev. B **90**, 205103 (2014).

[34] Y. Iqbal, P. Ghosh, R. Narayanan, B. Kumar, J. Reuther, and R. Thomale, Intertwined nematic orders in a frustrated ferromagnet, Phys. Rev. B **94**, 224403 (2016).

[35] A. Wietek and A. M. Läuchli, Sublattice coding algorithm and distributed memory parallelization for large-scale exact diagonalizations of quantum many-body systems, Phys. Rev. E **98**, 033309 (2018).

[36] A. M. Läuchli, J. Sudan, and E. S. Sørensen, Ground-state energy and spin gap of spin-$\frac{1}{2}$ kagomé-Heisenberg antiferromagnetic clusters: Large-scale exact diagonalization results, Phys. Rev. B **83**, 212401 (2011).

[37] See Supplemental Material at http://link.aps.org/supplemental/10.1103/PhysRevB.102.020411 for further information on the geometry of the lattice, its reciprocal lattice, and the naming convention of the representations of the space group.

[38] P. Lecheminant, B. Bernu, C. Lhuillier, L. Pierre, and P. Sindzingre, Order versus disorder in the quantum Heisenberg

antiferromagnet on the kagomé lattice using exact spectra analysis, Phys. Rev. B **56**, 2521 (1997).

[39] D. Poilblanc and G. Misguich, Competing valence bond crystals in the kagome quantum dimer model, Phys. Rev. B **84**, 214401 (2011).

[40] Y. Huh, M. Punk, and S. Sachdev, Vison states and confinement transitions of $\mathbb{Z}_2$ spin liquids on the kagome lattice, Phys. Rev. B **84**, 094419 (2011).

[41] K. Hwang, Y. Huh, and Y. B. Kim, $\mathbb{Z}_2$ gauge theory for valence bond solids on the kagome lattice, Phys. Rev. B **92**, 205131 (2015).

[42] K. Penc and A. M. Läuchli, Spin nematic phases in quantum spin systems, in *Introduction to Frustrated Magnetism*, edited by C. Lacroix, P. Mendels, and F. Mila, Springer Series in Solid-State Sciences Vol. 164 (Springer, Berlin, Heidelberg, 2010), Chap. 13.

[43] N. Shannon, T. Momoi, and P. Sindzingre, Nematic Order in Square Lattice Frustrated Ferromagnets, Phys. Rev. Lett. **96**, 027213 (2006).

[44] T. Momoi, P. Sindzingre, and N. Shannon, Octupolar Order in the Multiple Spin Exchange Model on a Triangular Lattice, Phys. Rev. Lett. **97**, 257204 (2006).

[45] T. Hikihara, L. Kecke, T. Momoi, and A. Furusaki, Vector chiral and multipolar orders in the spin-$\frac{1}{2}$ frustrated ferromagnetic chain in magnetic field, Phys. Rev. B **78**, 144404 (2008).

[46] J. Sudan, A. Lüscher, and A. M. Läuchli, Emergent multipolar spin correlations in a fluctuating spiral: The frustrated ferromagnetic spin-$\frac{1}{2}$ Heisenberg chain in a magnetic field, Phys. Rev. B **80**, 140402(R) (2009).

[47] Z. Hao, S. Inglis, and R. Melko, Destroying a topological quantum bit by condensing Ising vortices, Nat. Commun. **5**, 5781 (2014).

[48] A. Ralko, F. Mila, and I. Rousochatzakis, Microscopic theory of the nearest-neighbor valence bond sector of the spin-$\frac{1}{2}$ kagome antiferromagnet, Phys. Rev. B **97**, 104401 (2018).

[49] T. Senthil, A. Vishwanath, L. Balents, S. Sachdev, and M. P. A. Fisher, Deconfined quantum critical points, Science **303**, 1490 (2004).

[50] C.-M. Jian, A. Thomson, A. Rasmussen, Z. Bi, and C. Xu, Deconfined quantum critical point on the triangular lattice, Phys. Rev. B **97**, 195115 (2018).

[51] X.-Y. Song, C. Wang, A. Vishwanath, and Y.-C. He, Unifying description of competing orders in two-dimensional quantum magnets, Nat. Commun. **10**, 4254 (2019).